communications physics

ARTICLE

https://doi.org/10.1038/s42005-022-00992-2 OPEN

Topological triplet-superconductivity in spin-1 semimetal

GiBaik Sim[1,2], Moon Jip Park[1,3] & SungBin Lee[1✉]

Superconductivity in topological semimetals gives a new paradigm of unconventional superconductors. Their exotic gap structures and topological properties have fascinated searching for material realizations and applications. In this work, we focus on a triple point semimetal where quasiparticle excitations, triple point fermions, carry the effective integer spin-1 in two distinct valleys. Our work demonstrates that the triple point fermion stabilizes inter-valley *s*-wave spin-triplet pairing. This is due to Fermi statistics, which strictly forbids the formation of inter-valley *s*-wave spin-singlet pairings. This feature is clearly distinct from the BCS and other multi-band superconductors. We find that two distinct inter-valley *s*-wave spin-triplet superconductors are allowed which in principle can be controlled by tuning the chemical potential: time-reversal symmetric (s_z) state with topologically protected nodal lines and time-reversal broken ($s_x + is_y$) state with topologically protected Bogoliubov Fermi surfaces. Our study provides guidance in searching for spin-triplet superconductivity.

[1] Department of Physics, Korea Advanced Institute of Science and Technology, Daejeon 34141, Republic of Korea. [2] Department of Physics TQM, Technische Universität München, & James-Franck-Straße 1, D-85748 Garching, Germany. [3] Center for Theoretical Physics of Complex Systems, Institute for Basic Science (IBS), Daejeon 34126, Republic of Korea. ✉email: sungbin@kaist.ac.kr

The discovery of topological semimetallic phases has realized various types of quasiparticles, characterized by topologically non-trivial band crossings[1–11]. In particular, Bradlyn et al.[12] show that topological triple-band crossings are realizable in certain spin-orbit coupled materials. The quasiparticle excitations of such a band crossing are referred to as triple point fermions and carry the effective integer pseudospin $j = 1$. This peculiar spin structure of triple point fermions is possible because the condensed matter systems are not constrained by the fundamental spin-statistics theorem. It can have a major impact on the nature of the correlated ground states in the presence of many-body interactions. In particular, the possible occurrence of unconventional superconducting states calls for concrete theoretical understanding.

In general, Fermi statistics constrains the wavefunction of Cooper pairs to be anti-symmetric under the exchange of two identical electrons. As a result, the spatial parity and the spin part of the superconducting order parameter are not independent of each other[13]. For instance, if we consider a Cooper pair of spin $s = 1/2$ electrons in the conventional superconductors, the formation of even-parity (odd-parity) spin-singlet (spin-triplet), such as s-wave spin-singlet and p-wave spin-triplet, pairing is only allowed. This is due to the exchange symmetry of spin $s = 1/2$ electrons. The pseudospin $j = 1$ fermions have the opposite exchange symmetry of the spin $s = 1/2$ fermions. Thus, if we consider the pairing of the pseudospin $j = 1$ electrons, the spin-singlet (spin-triplet) selects the odd-parity (even-parity) pairing which is clearly distinct from BCS and other multi-band superconductors. This unique property of pseudospin $j = 1$ electrons motivates further investigation in the hunt for distinct forms of superconductivity.

In this work, we investigate s-wave spin-triplet superconducting ground states in an interacting triple point semimetal. We start from the low-energy Hamiltonian near the triple-band crossing points which can be realized in spin-orbit coupled materials with space group 199. Adopting the Landau theory, we establish the phase diagram of spin-triplet superconductivity in this system and demonstrate the realization of two distinct states; (i) (s_z) state with a rotational symmetry along the z direction and time-reversal symmetry. (ii) $(s_x + is_y)$ state with broken rotational and time-reversal symmetry. We find (s_z) state is energetically favored when the chemical potential lies far below the triple-band crossing point with the middle band having upward dispersion. In this case, the state contains nodal lines, which are topologically protected by the non-trivial winding number. On the other hand, when the chemical potential lies near or above the band crossing point, the system stabilizes the $(s_x + is_y)$ state. In this case, the Bogoliubov Fermi surface emerges whose non-trivial topological properties are revealed by calculating the Chern number. In the limit of a perfectly flat middle, the system selects the $(s_x + is_y)$ state regardless of other microscopic details. The unusual form of this spin-triplet superconductor is a generic feature of triple point fermions and can be controlled by tuning the chemical potential.

Results

Triple point fermions in spin-orbit coupled materials with space group 199. Bradlyn et al.[12] verify that spin-orbit coupled materials with time-reversal symmetry can realize topologically protected triple-band crossings. As a representative example, materials with space group 199 are demonstrated to host a pair of triple-band crossings at two inequivalent high symmetry points $\pm P$, which are time-reversal partners. Close to the band crossing points $\boldsymbol{q} = \pm \boldsymbol{K} + \boldsymbol{k}$, the Hamiltonian can be expanded up to the quadratic order as,

$$h_{\pm}(\boldsymbol{k}) = \psi^{\dagger}_{\pm,\boldsymbol{k}}[(ck^2 - \mu)\mathbb{I}_3 + v\boldsymbol{k}\cdot\boldsymbol{J}]\psi_{\pm,\boldsymbol{k}} \quad (1)$$

which displays $SO(3)$ and time-reversal symmetry. Note that we only include ck^2 among symmetry allowed quadratic terms, which preserves $SO(3)$ symmetry. Here, we define the three spinors as $\psi_{\pm,\boldsymbol{k}} = (\psi_{\pm,\boldsymbol{k},1}, \psi_{\pm,\boldsymbol{k},0}, \psi_{\pm,\boldsymbol{k},-1})$. The first subscript indicates the valley degree of freedom and the third subscript indicates the spin degree of freedom. $\boldsymbol{J} = (J_x, J_y, J_z)$ represents the $j = 1$ angular momentum matrices and $\mathbb{I}_3$ is the three-dimensional identity matrix. v and μ are the effective linear velocity of the band crossings and the chemical potential respectively. Inversion symmetry is broken in the case of finite v. The $c|\boldsymbol{k}|^2$ term represents a possible bending of bands and we assume $c > 0$ without loss of generality. The corresponding tight-binding model is given in Supplementary Note 1[14]. The Hamiltonian in Eq. (1) has two bands with the dispersion, $\epsilon^{\pm 1}(\boldsymbol{k}) = \pm v|\boldsymbol{k}| + c|\boldsymbol{k}|^2 - \mu$, having opposite spins, and the middle band with the dispersion, $\epsilon^0(\boldsymbol{k}) = c|\boldsymbol{k}|^2 - \mu$. These three bands can be characterized by the monopole charge of the Berry curvature, $C^{\pm 1} = \mp 2$ and $C^0 = 0$ respectively [12,15].

Possible pairing forms. Prior to the description of the interactions, we first discuss the generic form of the allowed inter-valley pairing order parameters for the above system. The pairing order parameters can be expressed as the sum of the bilinear form

$$\langle \psi^{\dagger}_{+,\boldsymbol{k}} Y_L(\boldsymbol{K} + \boldsymbol{k}) M_S \gamma \psi^{*}_{-,-\boldsymbol{k}} \rangle, \quad (2)$$

with spherical harmonics $Y_L(\boldsymbol{K} + \boldsymbol{k})$ describing the orbital part of the Cooper pair wavefunction. $\gamma = e^{-i\pi J_y}$ is the unitary part of the time-reversal operator $\mathcal{T} = \gamma\mathcal{K}$ ($\mathcal{K}$ is the complex conjugate operator). Here, $\boldsymbol{K}$ indicates the position of the valley + in momentum space and the spin pairing matrices M_S are the 3×3 multipole matrices of pseudospin $j = 1$ electrons and are listed in Table 1 (see Supplementary Note 2 for the explicit form of M_S). The exchange symmetry of pseudospin $j = 1$ electrons can be seen from the fact that $M_S\gamma$ with even (odd) S becomes symmetric (anti-symmetric) which is exactly the opposite pattern as in the case of electrons with half-integer spin.

The conjunction of the exchange symmetry and Fermi statistics selects specific sets of the pairing order parameters. Fermi statistics poses the relation: $Y_L(-\boldsymbol{K} - \boldsymbol{k})(M_S\gamma)^T = -Y_L(\boldsymbol{K} + \boldsymbol{k})M_S\gamma$. According to this condition, the even-parity pairings (even L) only allow spin-triplet ($S = 1$) pairing while the odd-parity pairings (odd L) allow spin-singlet ($S = 0$) and quintet ($S = 2$) pairings. As a result, the orbital part of the Cooper pair condensate, which carries the value of total spin $S = 1$, should be given by $Y_L(\boldsymbol{K} + \boldsymbol{k})$ with even L. The combination of the spatial parity and the total spin of the Cooper pair wavefunction displays exactly the opposite pattern from superconductors composed of electrons with half-integer spin. This is the key observation of our work. Here and below, we focus on inter-valley s-wave ($L = 0$) spin-triplet ($S = 1$) pairings. Other

Table 1 List of spin pairing matrices.

S	M_S	Spatial Parity
0	$\mathbb{I}_3$	Odd
1	$\sqrt{\frac{3}{2}}(J_x, J_y, J_z)$	Even
2	$(\Gamma_{x^2-y^2}, \Gamma_{3z^2-r^2}, \Gamma_{yz}, \Gamma_{zx}, \Gamma_{xy})$	Odd

Electrons with $j = 1$ can form a pair with the total spin $S = 0, 1, 2$. A Cooper pair with the total spin S is created by the operator $\psi^{\dagger}_{+,\boldsymbol{k}} Y_L(\boldsymbol{K} + \boldsymbol{k}) M_S \gamma \psi^{*}_{-,-\boldsymbol{k}}$ where L describes the orbital part of the Cooper pair. The spin and orbital part of the Cooper pair are not independent to each other: Since the spin pairing matrices $M_{S=1}\gamma$ are anti-symmetric, the corresponding orbital part should be described by $Y_L(\boldsymbol{K} + \boldsymbol{k})$ with even L. While $M_{S=0,2}\gamma$ should be additionally multiplied by $Y_L(\boldsymbol{K} + \boldsymbol{k})$ with odd L to satisfy Fermi statistics. The third column indicates the spatial parity of the corresponding superconducting order parameter.

types of pairing are considered in ref. [16–18] which include the intra-valley pairings (pair density wave states) and inter-valley d-wave ($L=2$) spin-singlet ($S=0$) pairings.

Two distinct *s*-wave spin-triplet paired states. We now consider the following form of the interaction,

$$h_{int} = g \sum_{a=x,y,z} (\psi^\dagger_{+,\boldsymbol{k}} J_a \psi_{+,\boldsymbol{k}'})(\psi^\dagger_{-,-\boldsymbol{k}} J_a \psi_{-,-\boldsymbol{k}'}). \quad (3)$$

These terms constitute a complete set of momentum independent interactions with $SO(3)$ symmetry[19] and we consider the repulsive interactions, $g>0$. In Supplementary Note 4, we consider microscopic symmetry allowed interactions, on site Hubbard repulsion and nearest neighbor interactions, and investigate whether they can provide the terms given in Eq. (3). It turns out that attractive spin independent nearest neighbor interactions and antiferromagnetic nearest neighbor interactions induce such repulsive interactions between triple point fermions. Eq. (3) can be exactly rewritten in the following way using Fierz identities for electrons with pseudospin $j=1$ (see Supplementary Note 3 for the details)[19–22].

$$h_{int} = -\frac{g}{2} \sum_{a=x,y,z} (\psi^\dagger_{+,\boldsymbol{k}} J_a \gamma \psi^*_{-,-\boldsymbol{k}})(\psi^T_{-,-\boldsymbol{k}'} (J_a\gamma)^\dagger \psi_{+,\boldsymbol{k}'}) \quad (4)$$

This means that there exists a superconducting instability even when the bare interactions are all repulsive ($g>0$). Based on the pairing terms given in Eq. (4), we now derive the Ginzburg–Landau(GL) free energy, $F(\vec{\Delta}, T, v, \mu, g)$, as a function of the order parameter, $\vec{\Delta} = (\Delta_x, \Delta_y, \Delta_z)$, where $\Delta_a = \langle \psi^T_{-,-\boldsymbol{k}} (J_a\gamma)^\dagger \psi_{+,\boldsymbol{k}} \rangle$ corresponds to the s-wave spin-triplet pair. By integrating out the electronic degrees of freedom, the free energy functional can be written as

$$\begin{aligned} F = {} & r(T,v,\mu,g)|\vec{\Delta}|^2 + q_1(T,v,\mu)|\vec{\Delta}|^4 \\ & + q_2(T,v,\mu) \sum_{a=1}^{3} |\vec{\Delta}^* \mathcal{I}_a \vec{\Delta}|^2, \end{aligned} \quad (5)$$

where the matrix elements of $\mathcal{I}_a$ are given as $(\mathcal{I}_a)_{bc} = i\epsilon_{abc}$ using the Levi-Civita symbol ϵ_{abc}[23,24]. We find that Eq. (5) can have the two possible superconducting ground states solely depending on the value of the coefficient q_2 in the weak pairing limit. When $q_2>0$, the time-reversal symmetric state with the order parameter $\vec{\Delta} = (0,0,1)$ is stabilized. For $q_2<0$ however, the time-reversal broken state is stabilized with the order parameter $\vec{\Delta} = (1,i,0)$. We note that distinct complex order parameters are physically equivalent if there exists *an* $SO(3)$ rotation that can transform one to the other. From now on, we label $\vec{\Delta} = (0,0,1)$ and $(1,i,0)$ states as (s_z) and (s_x+is_y) states respectively.

The (s_z) and (s_x+is_y) order parameters have distinct spin textures. The $M_S\gamma$ for (s_z) state is explicitly given by

$$J_z\gamma = \begin{pmatrix} 0 & 0 & 1 \\ 0 & 0 & 0 \\ -1 & 0 & 0 \end{pmatrix}. \quad (6)$$

From the explicit form of the matrix, we can observe that the (s_z) state forms Cooper pairs with opposite spin components, using inter-band pairing. On the other hand, the corresponding matrix for (s_x+is_y) state is written as

$$\frac{(J_x+iJ_y)\gamma}{\sqrt{2}} = \begin{pmatrix} 0 & -1 & 0 \\ 1 & 0 & 0 \\ 0 & 0 & 0 \end{pmatrix}. \quad (7)$$

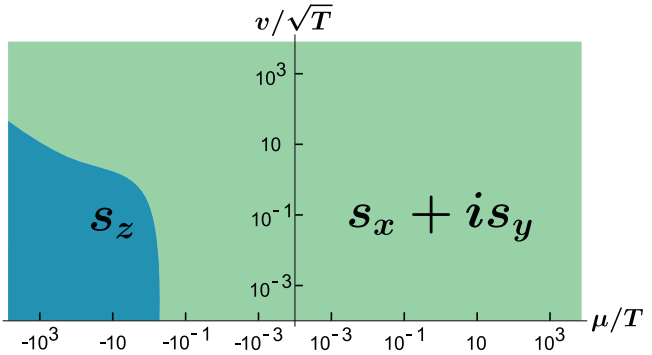

Fig. 1 Phase diagram of *s*-wave spin-triplet pairings. Within the leading one-loop calculation, triple point semimetals selectively stabilize two distinct paired states, depending on μ/T and $v/\sqrt{T}$: time-reversal symmetry broken state with (s_x+is_y) pairing (green) and time-reversal symmetric state with (s_z) pairing (blue). μ, T, and v indicate chemical potential, temperature, and effective linear velocity of the band crossings respectively.

For (s_x+is_y) state, if we consider an electron with $j_z=1$, it forms an inter-band pairing with ${}_a\, j_z=0$ electron. Similarly, (s_x-is_y) state pairs ${}_a\, j_z=-1$ electron with ${}_a\, j_z=0$ electron.

By explicitly investigating the sign of q_2 within the leading one-loop calculation, one can determine the energetically favored state (see Methods for details). Figure 1 shows the calculated phase diagram as a function of the dimensionless parameters, μ/T and $v/\sqrt{T}$, while fixing a dimensionless parameter $c=1/10$ with the momentum cutoff $\Lambda=\mu/v$. First of all, when the chemical potential lies far below the band crossing point, we find that the (s_z) state is favored preserving time-reversal symmetry. However, when the chemical potential approaches the band crossing point, the contribution of the middle band to the free energy becomes significant. We find that the (s_x+is_y) pairing is stabilized when the chemical potential lies near or above the band crossing point. In the limit where the middle band is perfectly flat ($c=0$), our one-loop calculation with momentum cutoff $\Lambda=\mu/v$ shows that q_2 is always negative, favoring the (s_x+is_y) state (see Methods for details).

Gap structures and topological properties. After constructing the Landau theory and phase diagram of the system, we now discuss the Bogoliubov-de Gennes (BdG) quasiparticle spectrum of the superconducting states. The BdG Hamiltonian reads $\sum_{\boldsymbol{k}} \Psi^\dagger_{\boldsymbol{k}} H_{BdG}(\boldsymbol{k}) \Psi_{\boldsymbol{k}}$ with

$$H_{BdG}(\boldsymbol{k}) = \begin{pmatrix} \hat{h}(\boldsymbol{k}) & \hat{\Delta} \\ \hat{\Delta}^\dagger & -\hat{h}^T(-\boldsymbol{k}), \end{pmatrix} \quad (8)$$

where $\Psi^\dagger_{\boldsymbol{k}} = (\psi^\dagger_{+,\boldsymbol{k}}, \psi_{-,-\boldsymbol{k}})$ and $\hat{h}(\boldsymbol{k}) = (ck^2-\mu)\mathbb{I}_3 + v\boldsymbol{k}\cdot\boldsymbol{J}$. Here, $\hat{\Delta} = |\Delta| J_z\gamma$ for the (s_z) state and $\hat{\Delta} = |\Delta|(J_x+iJ_y)\gamma$ for the (s_x+is_y) state, where Δ is a real constant. For the time-reversal symmetric superconductor with (s_z) pairing, $H_{BdG}(\boldsymbol{k})$ belongs to class BDI[25] and the spectrum is derived using a singular value decomposition of the matrix $\hat{h}(\boldsymbol{k}) + i|\Delta|J_z = v(k_x,k_y,k_z+i|\Delta|)\cdot\boldsymbol{J} + (ck^2-\mu)\mathbb{I}_3$. The corresponding eigenvalues are given by

$$\lambda_{s=1,0,-1}(\boldsymbol{k}) = c|\boldsymbol{k}|^2 - \mu + s\sqrt{v^2|\boldsymbol{k}|^2 - |\Delta|^2 + 2i|\Delta|k_z}. \quad (9)$$

For the momentum point $\boldsymbol{k}$ where $\lambda_s(\boldsymbol{k})=0$ is satisfied, the BdG energy spectrum become gapless. We find that $\lambda_{\pm1}(\boldsymbol{k})=0$ if $k_z=0$ and $c|\boldsymbol{k}|^2-\mu = \mp\sqrt{v^2|\boldsymbol{k}|^2-|\Delta|^2}$. These conditions define the two nodal lines when $\mu > c\Delta^2/v^2 - v^2/4c$. Figure 2a shows the two nodal rings which are represented by solid and

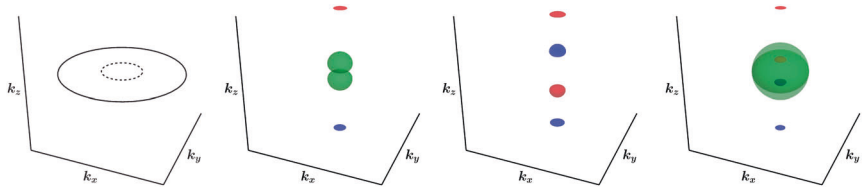

(a) (s_z) state with $\mu<0$ (b) (s_x+is_y) state with $\mu<0$ (c) (s_x+is_y) state with $\mu=0$ (d) (s_x+is_y) state with $\mu>0$

Fig. 2 Gap structure of the superconducting states. a (s_z) state with the chemical potential $\mu<0$ − A solid(dashed) ring indicates the nodal ring which is protected by the non-trivial winding number 1(− 1). Each gapless region in (s_z) state have two-fold degeneracy protected by the chiral symmetry (**b**) (s_x+is_y) state with $\mu<0$, (**c**) (s_x+is_y) state with $\mu=0$, and **d** (s_x+is_y) state with $\mu>0$ − Each surface indicates the non-degenerate Bogoliubov Fermi surface and the color represents its Chern number. Green, red, and blue indicates 0, −1, and 1, respectively.

dashed lines. The nodal rings are topologically protected by a non-trivial winding number, $\omega\in\mathbb{Z}$, thus they are stable against any symmetry preserving perturbations. The winding number can be calculated as $\omega=\frac{1}{2\pi}\sum_s\int_0^{2\pi}\partial_\theta\arg(\lambda_s)$, where the integration is taken over the loop that encircles each nodal line[25,26]. We immediately find that the winding number of each solid and dashed nodal line is 1 and − 1 respectively. Similarly, the condition $\lambda_0(\boldsymbol{k})=0$ defines the nodal surface, often referred to as Bogoliubov Fermi surface[27–36]. Unlike the nodal lines, the Bogoliubov Fermi surface, characterized by $\lambda_0(\boldsymbol{k})=0$, is topologically trivial. This can be seen by including the additional odd-parity spin-singlet superconducting order parameter, which instantly gaps out the system. As a consequence, we expect to find topologically stable nodal lines for the time-reversal symmetric (s_z) phase.

We now consider the gap structure of the time-reversal broken (s_x+is_y) state. In this case our system belongs to class D[25] and the gapless region can be calculated by finding $\boldsymbol{k}$ points which satisfy $\det[H_{BdG}(\boldsymbol{k})]=0$. This condition can be rewritten as

$$4|\Delta|^2(|\Delta|^2+\bar{\mu}^2)(v^2k_z^2-\bar{\mu}^2)=\bar{\mu}^2(v^2|\boldsymbol{k}|^2-\bar{\mu}^2)^2, \qquad (10)$$

where $\bar{\mu}=ck^2-\mu$. This condition generally defines the surface in three-dimensional momentum space. It realizes the nodal surface in the BdG energy spectrum (See Fig. 2b–d). This Bogoliubov Fermi surface can be characterized by two distinct topological invariants[25]. The first is the $\mathbb{Z}_2$ valued number of occupied BdG bands. Each Bogoliubov Fermi surface is non-degenerate since time-reversal symmetry is absent. This indicates that these surfaces are all topologically protected as the $\mathbb{Z}_2$ number always changes by 1 when the energy level crosses a single Bogoliubov Fermi surface in the momentum space. The presence of a non-trivial $\mathbb{Z}_2$ number means that each Bogoliubov Fermi surface is locally stable until two surfaces pair-annihilate. In addition to the $\mathbb{Z}_2$ number, the surface can be also characterized by a non-trivial Chern number[29,37]. In Fig. 2b–d, the Bogoliubov Fermi surface with Chern number $1(-1)$ is colored blue(red). Rather than simply presenting the numerical results, we argue that the non-trivial Chern number is a necessary consequence of the well-known parity anomaly for two-dimensional Dirac fermions[38,39]. First of all, we consider the adiabatic change from the (s_x) state to the (s_x+is_y) state by slightly turning on an (s_y) pairing. In the (s_x) state, the $k_z=0$ plane can be viewed as a nodal point superconductor with two Dirac nodal points per Bogoliubov Fermi surface. These Dirac nodal points are pinned to the zero energy states and they are time-reversal partners to one another. As the infinitesimal time-reversal symmetry breaking (s_y) pairing is turned on, the two Dirac points gaps out and must carry the Chern number ± 1/2, which is analogous to the parity anomaly for two-dimensional Dirac fermions. Since the time-reversal symmetry is broken, the effective mass gap of two Dirac points must be opposite to one another, therefore the $k_z=0$ plane must be characterized by a non-trivial Chern number. As a consequence, in full three-dimensional momentum space, each topologically protected nodal line is inflated into a couple of Bogoliubov Fermi surfaces possessing non-trivial Chern number ± 1. In principle, the inflation occurs for each nodal line, and the total Chern number at the $k_z=0$ plane can vanish. However, each Bogoliubov Fermi surface must carry a non-trivial Chern number until they pair-annihilate.

Discussion

In conclusion, we have studied the spin-triplet superconductivity of triple point fermions which are described by a pseudospin-1 representation. In the superconductor composed of pseudospin $j=1$ electrons, Cooper pairs which are even in spatial parity should carry total spin $S=1$. Furthermore, we have shown that multi-band interactions open attractive inter-valley spin-triplet pairing channels. Based on Landau theory, we find two distinct inter-valley spin-triplet superconducting phases depending on the chemical potential μ: the time-reversal symmetric (s_z) state and the time-reversal broken (s_x+is_y) state. In particular, (s_x+is_y) phase is favored when the chemical potential lies near or above the triple-band crossing point in such a way that the middle band plays a role in electron pairing. Moreover, we find that the two states can be distinguished by the dimension of nodes and their topological characteristics. Hence, we suggest that the spin-triplet superconductor is naturally stabilized in triple point semimetals with momentum independent interactions. To illustrate our general idea, we also present an example of triple point fermions in spin-orbit coupled materials with space group 199 and derive the microscopic mechanism for the realization of inter-valley spin-triplet superconductors. In general, the superconducting instability is not limited to momentum independent interactions, and therefore one may expect odd-parity superconductivity in the presence of momentum dependent interactions. In this case, we may expect the formation of p-wave spin-singlet and quintet pairing states. The investigation of possible odd-parity superconductivity would be an interesting topic for future study.

Methods

Ginzburg–Landau free energy and one-loop calculation. Here, we compute the coefficients of Ginzburg–Landau free energy $F(\vec{\Delta})$. We first introduce the propagator

$$G(K)=(ik_0+(ck^2-\mu)\mathbb{I}_3+v\boldsymbol{k}\cdot\boldsymbol{J})^{-1}. \qquad (11)$$

Here $K \equiv (k_0, \boldsymbol{k})$ and $k_0 = 2\pi(n+1/2)T$ denotes Matsubara frequency. Then, the free energy is written as

$$F(\overrightarrow{\Delta}) = \frac{1}{g}|\overrightarrow{\Delta}|^2 + T\sum_{m,n}\int_{|\boldsymbol{k}|\le\Lambda}\frac{1}{2m}\,\mathrm{tr}\,(-G(K)\Delta G(-K)^T\Delta^\dagger)^m \mathrm{d}^3k, \tag{12}$$

where we introduce a momentum cutoff Λ and $\Delta = \sum_a J_a\gamma\Delta_a$. Let $F_n(\overrightarrow{\Delta})$ be the contribution to the free energy that contains n-th power of Δ_a. We have

$$F_2(\overrightarrow{\Delta}) = \frac{1}{g}|\overrightarrow{\Delta}|^2 - \frac{1}{2}\sum_{a,b}L_{ab}\Delta_a\Delta_b^*, \tag{13}$$

$$F_4(\overrightarrow{\Delta}) = \frac{1}{4}\sum_{a,b,c,d}L_{abcd}\Delta_a\Delta_b^*\Delta_c\Delta_d^* \tag{14}$$

with

$$L_{ab} = T\sum_n\int_{|\boldsymbol{k}|\le\Lambda}\mathrm{tr}\,(G(K)J_a\gamma G(-K)^T(J_a\gamma)^\dagger)\mathrm{d}^3k, \tag{15}$$

$$\begin{aligned}L_{abcd} = T\sum_n\int_{|\boldsymbol{k}|\le\Lambda}&\mathrm{tr}\,\big(G(K)J_a\gamma G(-K)^T(J_b\gamma)^\dagger\\&\times G(K)J_c\gamma G(-K)^T(J_d\gamma)^\dagger\big)\mathrm{d}^3k.\end{aligned} \tag{16}$$

Meanwhile, we can parametrize the general terms in $F_n(\overrightarrow{\Delta})$ accordingly.

$$F_2(\overrightarrow{\Delta}) = r|\overrightarrow{\Delta}|^2, \tag{17}$$

$$F_4(\overrightarrow{\Delta}) = q_1|\overrightarrow{\Delta}|^4 + q_2\sum_a|\overrightarrow{\Delta}^*\mathcal{I}_a\overrightarrow{\Delta}|^2 \tag{18}$$

where the matrix elements of $\mathcal{I}_a$ is given as $(\mathcal{I}_a)_{bc} = i\epsilon_{abc}$ and ϵ_{abc} is the Levi-Civita symbol. Taking the specific configurations

$$\overrightarrow{\Delta}^1 = (0,0,1),\ \overrightarrow{\Delta}^2 = \frac{1}{\sqrt{2}}(1,i,0) \tag{19}$$

we apply Eq.(14) and

$$F_4(\overrightarrow{\Delta}^1) = q_1, F_4(\overrightarrow{\Delta}^2) = q_1 + q_2 \tag{20}$$

to get the coefficients q_1 and q_2. With introducing $\hat{k}_0 = k_0/T, \hat{k} = k/\sqrt{T}, \hat{\mu} = \mu/T$, $\hat{v} = v/\sqrt{T}$, and $\hat{\Lambda} = \hat{\mu}/\hat{v}$ we find

$$\begin{aligned}q_1 = \frac{1}{T^{3/2}}\sum_n\int_0^{\hat{\Lambda}}\Big[g_1\Big(&((\hat{\mu}-c\hat{k}^2)^2+\hat{k}_0^2)^2((\hat{k}(\hat{v}-c\hat{k})+\hat{\mu})^2+\hat{k}_0^2)^2\\&\times((\hat{\mu}-\hat{k}(c\hat{k}+\hat{v}))^2+\hat{k}_0^2)^2\Big)^{-1}\Big]\hat{k}^2\mathrm{d}\hat{k}\end{aligned} \tag{21}$$

$$\begin{aligned}q_2 = \frac{1}{T^{3/2}}\sum_n\int_0^{\hat{\Lambda}}\Big[g_2\Big(&((\hat{\mu}-c\hat{k}^2)^2+\hat{k}_0^2)^2((\hat{k}(\hat{v}-c\hat{k})+\hat{\mu})^2+\hat{k}_0^2)^2\\&\times((\hat{\mu}-\hat{k}(c\hat{k}+\hat{v}))^2+\hat{k}_0^2)^2\Big)^{-1}\Big]\hat{k}^2\mathrm{d}\hat{k}\end{aligned} \tag{22}$$

where

$$\begin{aligned}g_1 = \frac{2}{15}\pi\Big((\hat{\mu}-c\hat{k}^2)^4&\big(15c^4\hat{k}^8+10c^2\hat{k}^6\hat{v}^2+10\hat{k}^2\hat{\mu}^2(9c^2\hat{k}^2+\hat{v}^2)\\&-20c\hat{k}^4\hat{\mu}(3c^2\hat{k}^2+\hat{v}^2)-60c\hat{k}^2\hat{\mu}^3-\hat{k}^4\hat{v}^4+15\hat{\mu}^4\big)\\&+5\hat{k}_0^2\big(2(\hat{\mu}-c\hat{k}^2)^2\big(6c^4\hat{k}^8-24c^3\hat{k}^6\hat{\mu}+c^2(5\hat{k}^6\hat{v}^2+36\hat{k}^4\hat{\mu}^2)\\&-2c(5\hat{k}^4\hat{\mu}\hat{v}^2+12\hat{k}^2\hat{\mu}^3)-5\hat{k}^4\hat{v}^4+5\hat{k}^2\hat{\mu}^2\hat{v}^2+6\hat{\mu}^4\big)\\&+\hat{k}_0^2\Big(18c^4\hat{k}^8-72c^3\hat{k}^6\hat{\mu}+2c^2(7\hat{k}^6\hat{v}^2+54\hat{k}^4\hat{\mu}^2)\\&-4c(7\hat{k}^4\hat{\mu}\hat{v}^2+18\hat{k}^2\hat{\mu}^3)+3\hat{k}^4\hat{v}^4+14\hat{k}^2\hat{\mu}^2\hat{v}^2+18\hat{\mu}^4\\&+3\hat{k}_0^2\big(4c^2\hat{k}^4-8c\hat{k}^2\hat{\mu}+2\hat{k}^2\hat{v}^2+\hat{k}_0^2+4\hat{\mu}^2\big)\big)\Big)\big),\end{aligned} \tag{23}$$

$$\begin{aligned}g_2 = \frac{2}{15}\pi\hat{k}^2\hat{v}^2\Big(&(\hat{\mu}-c\hat{k}^2)^2\big(5c^4\hat{k}^8-20c^3\hat{k}^6\hat{\mu}+6c^2\hat{k}^4(5\hat{\mu}^2-3\hat{k}^2\hat{v}^2)\\&+4c\big(9\hat{k}^4\hat{\mu}\hat{v}^2-5\hat{k}^2\hat{\mu}^3\big)+5\hat{k}^4\hat{v}^4-18\hat{k}^2\hat{\mu}^2\hat{v}^2+5\hat{\mu}^4\big)\\&+5\hat{k}_0^2\Big(c^4\hat{k}^8-4c^3\hat{k}^6\hat{\mu}+c^2(6\hat{k}^4\hat{\mu}^2-4\hat{k}^6\hat{v}^2)+c(8\hat{k}^4\hat{\mu}\hat{v}^2-4\hat{k}^2\hat{\mu}^3)\\&-\hat{k}^4\hat{v}^4-4\hat{k}^2\hat{\mu}^2\hat{v}^2+\hat{\mu}^4\\&-\hat{k}_0^2\big(c^2\hat{k}^4-2c\hat{k}^2\hat{\mu}+2\hat{k}^2\hat{v}^2+\hat{k}_0^2+\hat{\mu}^2\big)\Big)\Big).\end{aligned} \tag{24}$$

Utilizing Eqs.(22) and (24), we investigate the sign of q_2 varying $\hat{\mu}$ and $\hat{v}$ while keeping $c = 1/10$. Then we acquire the phase diagram as given in Fig. 1.

In the limit where the middle band is perfectly flat($c = 0$), q_1 and q_2 can be simplified as below with normalizing the field ψ such that $\hat{v}$ becomes unity.

$$\begin{aligned}q_1 = \frac{1}{T^{3/2}}\frac{2\pi}{15}\sum_n\int_0^{\hat{\mu}}\Big[&10\hat{k}^2(\hat{k}_0^2+\hat{\mu}^2)^2(3\hat{k}_0^2+\hat{\mu}^2)+15(\hat{k}_0^2+\hat{\mu}^2)^4\\&+\hat{k}^4\big(-50\hat{k}_0^2\hat{\mu}^2+15\hat{k}_0^4-\hat{\mu}^4\big)\Big]\Big[\big(\hat{k}_0^2+\hat{\mu}^2\big)^2\big((\hat{\mu}-\hat{k})^2+\hat{k}_0^2\big)^2\\&\times\big((\hat{k}+\hat{\mu})^2+\hat{k}_0^2\big)^2\Big]^{-1}\hat{k}^2\mathrm{d}\hat{k},\end{aligned} \tag{25}$$

$$\begin{aligned}q_2 = \frac{1}{T^{3/2}}\frac{2\pi}{15}\sum_n\int_0^{\hat{\mu}}\Big[&\hat{k}^2\big(5\hat{k}^4\hat{\mu}^2-18\hat{k}^2\hat{\mu}^4-5\hat{k}_0^2\big(\hat{k}^4+4\hat{k}^2\hat{\mu}^2\\&+\hat{k}_0^2\big(2\hat{k}^2+\hat{\mu}^2\big)+\hat{k}_0^4-\hat{\mu}^4\big)+5\hat{\mu}^6\big)\Big]\Big[\big(\hat{k}_0^2+\hat{\mu}^2\big)^2\big((\hat{\mu}-\hat{k})^2+\hat{k}_0^2\big)^2\\&\times\big((\hat{k}+\hat{\mu})^2+\hat{k}_0^2\big)^2\Big]^{-1}\hat{k}^2\mathrm{d}\hat{k}\end{aligned} \tag{26}$$

We observe that the free energy is stable ($q_1T^{3/2} > 0$) and time-reversal broken phase is energetically favored ($q_2T^{3/2} < 0$) when the middle band is perfectly flat ($c = 0$).

Data availability

The data that support the findings of this study are available from the corresponding author upon reasonable request.

Code availability

The code used to generate the data used in this study is available from the corresponding author upon reasonable request.

Received: 10 October 2020; Accepted: 8 August 2022;
Published online: 07 September 2022

References

1. Soluyanov, A. A. et al. Type-II Weyl semimetals. *Nature* **527**, 495 (2015).
2. Muechler, L., Alexandradinata, A., Neupert, T. & Car, R. Topological nonsymmorphic metals from band inversion. *Phys. Rev. X* **6**, 041069 (2016).
3. Wang, Z., Alexandradinata, A., Cava, R. J. & Bernevig, B. A. Hourglass fermions. *Nature* **532**, 189 (2016).
4. Burkov, A., Hook, M. & Balents, L. Topological nodal semimetals. *Phys. Rev. B* **84**, 235126 (2011).
5. Kim, Y., Wieder, B. J., Kane, C. & Rappe, A. M. Dirac line nodes in inversion-symmetric crystals. *Phys. Rev. Lett.* **115**, 036806 (2015).
6. Bzdušek, T., Wu, Q., Rüegg, A., Sigrist, M. & Soluyanov, A. A. Nodal-chain metals. *Nature* **538**, 75 (2016).
7. Wieder, B. J., Kim, Y., Rappe, A. & Kane, C. Double Dirac semimetals in three dimensions. *Phys. Rev. Lett.* **116**, 186402 (2016).
8. Chang, G. et al. Unconventional chiral fermions and large topological Fermi arcs in RhSi. *Phys. Rev. Lett.* **119**, 206401 (2017).
9. Chang, G. et al. Topological quantum properties of chiral crystals. *Nat. Mater.* **17**, 978 (2018).
10. Zhu, Z., Winkler, G. W., Wu, Q., Li, J. & Soluyanov, A. A. Triple point topological metals. *Phys. Rev. X* **6**, 031003 (2016).
11. Cano, J., Bradlyn, B. & Vergniory, M. Multifold nodal points in magnetic materials. *APL Mater.* **7**, 101125 (2019).
12. Bradlyn, B. et al. Beyond Dirac and Weyl fermions: Unconventional quasiparticles in conventional crystals. *Science* **353**, aaf5037 (2016).
13. Sigrist, M. & Ueda, K. Phenomenological theory of unconventional superconductivity. *Rev. Mod. Phys.* **63**, 239 (1991).
14. Po, H. C., Watanabe, H., Zaletel, M. P. & Vishwanath, A. Filling-enforced quantum band insulators in spin-orbit coupled crystals. *Sci. Adv.* **2**, e1501782 (2016).
15. Lin, Y.-P. & Hsiao, W.-H. Dual haldane sphere and quantized band geometry in chiral multifold fermions. *Phys. Rev. B* **103**, L081103 (2021).
16. Lin, Y.-P. & Nandkishore, R. M. Exotic superconductivity with enhanced energy scales in materials with three band crossings. *Phys. Rev. B* **97**, 134521 (2018).
17. Lin, Y.-P. Chiral flat band superconductivity from symmetry-protected three-band crossings. *Phys. Rev. Res.* **2**, 043209 (2020).

18. Mandal, S., Link, J. M. & Herbut, I. F. Time-reversal symmetry breaking and d-wave superconductivity of triple-point fermions. *Phys. Rev. B* **104**, 134512 (2021).
19. Herbut, I. F. Hidden role of antiunitary operators in Fierz transformation. *Phys. Rev. D* **100**, 116015 (2019).
20. Vafek, O. Interacting fermions on the honeycomb bilayer: From weak to strong coupling. *Phys. Rev. B* **82**, 205106 (2010).
21. Herbut, I. F. & Janssen, L. Topological Mott insulator in three-dimensional systems with quadratic band touching. *Phys. Rev. Lett.* **113**, 106401 (2014).
22. Boettcher, I. & Herbut, I. F. Anisotropy induces non-Fermi-liquid behavior and nematic magnetic order in three-dimensional Luttinger semimetals. *Phys. Rev. B* **95**, 075149 (2017).
23. Ho, T.-L. Spinor Bose condensates in optical traps. *Phys. Rev. Lett.* **81**, 742 (1998).
24. Venderbos, J. W., Savary, L., Ruhman, J., Lee, P. A. & Fu, L. Pairing states of spin-$\frac{3}{2}$ fermions: symmetry-enforced topological gap functions. *Phys. Rev. X* **8**, 011029 (2018).
25. Schnyder, A. P., Ryu, S., Furusaki, A. & Ludwig, A. W. Classification of topological insulators and superconductors in three spatial dimensions. *Phys. Rev. B* **78**, 195125 (2008).
26. Qi, X.-L., Hughes, T. L. & Zhang, S.-C. Topological invariants for the Fermi surface of a time-reversal-invariant superconductor. *Phys. Rev. B* **81**, 134508 (2010).
27. Agterberg, D., Brydon, P. & Timm, C. Bogoliubov fermi surfaces in superconductors with broken time-reversal symmetry. *Phys. Rev. Lett.* **118**, 127001 (2017).
28. Timm, C., Schnyder, A., Agterberg, D. & Brydon, P. Inflated nodes and surface states in superconducting half-Heusler compounds. *Phys. Rev. B* **96**, 094526 (2017).
29. Brydon, P., Agterberg, D., Menke, H. & Timm, C. Bogoliubov Fermi surfaces: General theory, magnetic order, and topology. *Phys. Rev. B* **98**, 224509 (2018).
30. Yuan, N. F. & Fu, L. Zeeman-induced gapless superconductivity with a partial Fermi surface. *Phys. Rev. B* **97**, 115139 (2018).
31. Oh, H. & Moon, E.-G. Instability of $j = \frac{3}{2}$ bogoliubov fermi surfaces. *Phys. Rev. B* **102**, 020501 (2020).
32. Link, J. M., Boettcher, I. & Herbut, I. F. *d*-wave superconductivity and Bogoliubov-Fermi surfaces in Rarita-Schwinger-Weyl semimetals. *Phys. Rev. B* **101**, 184503 (2020).
33. Link, J. M. & Herbut, I. F. Bogoliubov-fermi surfaces in noncentrosymmetric multicomponent superconductors. *Phys. Rev. Lett.* **125**, 237004 (2020).
34. Setty, C., Bhattacharyya, S., Cao, Y., Kreisel, A. & Hirschfeld, P. Topological ultranodal pair states in iron-based superconductors. *Nature communications* **11**, 523 (2020).
35. Sim, G. et al. Topological $d + s$ wave superconductors in a multiorbital quadratic band touching system. *Physical Review B* **100**, 064509 (2019).
36. Sim, G. et al. Multipolar superconductivity in Luttinger semimetals. *Physical Review Research* **2**, 023416 (2020).
37. Bzdušek, T. & Sigrist, M. Robust doubly charged nodal lines and nodal surfaces in centrosymmetric systems. *Physical Review B* **96**, 155105 (2017).
38. Fradkin, E., Dagotto, E. & Boyanovsky, D. Physical realization of the parity anomaly in condensed matter physics. *Physical review letters* **57**, 2967 (1986).
39. Burkov, A. Quantum anomalies in nodal line semimetals. *Physical Review B* **97**, 165104 (2018).

Acknowledgements

We thank Daniel Agterberg, Jennifer Cano, Gil Young Cho, and Yong Baek Kim for the valuable discussions. This work is supported by the National Research Foundation Grants (NRF- 2020R1A4A3079707, NRF- 2021R1A2C1093060). G.B.S. is funded by the European Research Council (ERC) under the European Unions Horizon 2020 research and innovation program (grant agreement No. 771537). M.J.P. acknowledge financial support from the Institute for Basic Science in the Republic of Korea through the project IBS-R024-D1. S.B.L. thanks the hospitality at the Physics Department of University of California, San Diego.

Author contributions

The research reported in the manuscript was carried out by G.B.S. and M.J.P. under the supervision of S.B.L.

Competing interests

The authors declare no competing interests.

Additional information

Supplementary information The online version contains supplementary material available at https://doi.org/10.1038/s42005-022-00992-2.

Correspondence and requests for materials should be addressed to SungBin Lee.

Peer review information *Communications Physics* thanks the anonymous reviewers for their contribution to the peer review of this work.

Reprints and permission information is available at http://www.nature.com/reprints

Publisher's note Springer Nature remains neutral with regard to jurisdictional claims in published maps and institutional affiliations.